Microstructural Modeling and Multiscale Mechanical Properties Analysis of Cancellous Bone

Zhiqiang Huang[1, 2], Yufeng Nie[1, *] and Yiqiang Li[1]

Abstract: This paper is devoted to the microstructure geometric modeling and mechanical properties computation of cancellous bone. The microstructure of the cancellous bone determines its mechanical properties and a precise geometric modeling of this structure is important to predict the material properties. Based on the microscopic observation, a new microstructural unit cell model is established by introducing the Schwarz surface in this paper. And this model is very close to the real microstructure and satisfies the main biological characteristics of cancellous bone. By using the unit cell model, the multiscale analysis method is newly applied to predict the mechanical properties of cancellous bone. The effective stiffness parameters are calculated by the up-scaling multi-scale analysis. And the distribution of microscopic stress in cancellous bone is determined through the down-scaling procedure. In addition, the effect of porosity on the stiffness parameters is also investigated. The predictive mechanical properties are in good agreement with the available experimental results, which verifies the applicability of the proposed unit cell model and the validness of the multiscale analysis method to predict the mechanical properties of cancellous bone.

Keywords: Cancellous bone, microstructural modeling, multiscale analysis, stiffness parameters, stress distribution.

1 Introduction

Bone is a natural multifunctional biological material that presents a well-defined hierarchical structure. One of its important functions is to serve as a structural support for other tissues in the body [Hamed, Lee and Jasiuk (2010)]. As a connective tissue, bone is made of compact cortical bone, forming a hard outer layer, and porous cancellous bone, filling the interior spaces and ends of long bones [Arabnejad, Khanoki and Pasini (2013)]. In recent years, the investigation of the effective properties of cancellous bone is an important topic in biomechanics, and it is especially intensive as the requirement for clinical practice. For example, it was used to assess the effect on mechanical properties of bone diseases [Basaruddin, Takano and Nakano (2015)] and design the synthetic bone substitutes, especially is of importance in orthopedics for analyzing implants [Jaziri, Rahmoun, Naceur et al. (2012)].

---

[1] Research Center for Computational Science, Northwestern Polytechnical University, Xi'an, 710072, China.

[2] School of Applied Science, Taiyuan University of Science and Technology, Taiyuan, 030024, China.

[*] Corresponding Author: Yufeng Nie. Email: yfnie@nwpu.edu.cn.

To understand the mechanical and biological functions of the cancellous bone, it is essential to clarify the relationships between the mechanical properties and the structural changes at the microstructural level. This knowledge is important to analyze implants and manufacturing synthetic bone substitutes. In addition, it provides a guide in designs of novel artificial biomimetic materials for biomedical engineers [Hamed, Lee and Jasiuk (2010)]. For investigation of the cancellous bone properties, two kinds of approach have been developed, one is experimental methods, among which the dual X-ray absorptiometry and the quantitative ultrasonic technique are mostly used [Ilic, Hackl and Gilbert (2009)], and the other one concentrate upon developing a convenient mathematical model.

Last two decades, the geometry structure of the unit cell in cancellous bone has advanced a lot. Due to complicated geometry structure of cancellous bone, different models of the unit cell were proposed, most of them were proposed by describing the cancellous bone using the terms "rod-like" or "plate-like" for a subjective classification of cancellous bone. The unit cell was described as a cubic form [Mcelhaney (1970)], and the relationship between bone density and Young's modulus of cancellous bone was predicted. The unit cell was assumed as a domain with spherical cavity [Beaupre and Hayes (1985)].The unit cell also have described as a cubic form with fixed side length [Ilic, Hackl and Gilbert (2009)], where the solid frame was modeled as a system of thin walls with variable thickness and width. A parameterized microstructural unit cell model was presented based on the Schwarz surface [Huang, Nie, Yang et al. (2017)]. The other kinds of unit cells were also used, such as Bar-Net model, Plate-Frame-Hole model, Honeybomb model, Plate-bar model, etc.

In the aspect of numerical simulation, the rush development of computer technology gives a new chance to the bone research, the delicacy analysis and quantitative analysis can be easily implemented. Various analytical and computational models have been proposed to predict mechanical properties of bone at different structural scales. In fact, at the nanostructural level, bone is predominantly considered as a composite material composed of collagen matrix and reinforcing hydroxyapatite inclusions. Hosokawa [Hosokawa (2006)] used the finite-difference time-domain method to simulate biphasic materials using the purely viscoelastic theory and Biot's theory. Ilic et al. [Ilic, Hackl and Gilbert (2009)] has established the application of multiscale finite element method to model cancellous bone as an alternative to Biot's model. Podshivalov et al. [Podshivalov, Fischer and Bar-Yoseph (2011)] presented the 3D multiscale finite element analysis of trabecular bone, which can provide physicians a digital magnifying glass to facilitate continuous transition between macro- and micro-scales. Hamed [Hamed (2010)] predicted analytically the effective elastic constants of cortical bone by modeling its elastic response at different scales. Jaziri et al. [Jaziri, Rahmoun, Naceur et al. (2012)] proposed an elastoplastic damage coupled model for modelling of trabecular bone behavior, where the damage was carried out by limit analysis based on the MCK criterion. The effects of deteriorated trabecular bone structure on bone stiffness and strength were demonstrated by using 3D printing model [Barak and Black (2018)]. Mechanical properties of periodic interpenetrating phase composites were investigated to novel architected microstructures [Al-Ketan, Assad, Rashid et al. (2017)]. Sansalone et al. [Sansalone, Naili and Desceliers (2014)] developed a methodology which couple modeling and micromechanical homogenization to estimate the material properties of bone while taking into account the

uncertainties of the micro- and nanostructure of bone. Research on model parameters, sensitivity analysis has been applied to identify the key input parameters influencing the model output [Vu-Bac, Silani, Lahmer et al. (2015); Khader, Hamid, Zhuang et al. (2018)].

The cancellous bone is a bio-composite material owning several levels of hierarchical organization, and the multiscale FE approach is a promising methodology for geometric modeling and mechanical analysis of cancellous bone. The homogenization of heterogeneous materials with the use of multi-scale technique is a common method, and multi-scale finite element analysis is essential for efficient and reliable mechanical analysis of bone structure. Many previous multi-scale methods utilize multi-step homogenization for analysis of bone micro-structure [Fritsch (2009); Nikolov and Raabe (2008)], but they only considered the first-order asymptotic expansions. The second-order two-scale (SOTS) analysis method was introduced [Cui, Shin and Wang (1999)] to predict the physical and mechanical properties of periodic composites [Cui and Yu (2006); Yang, Cui, Nie et al. (2012)]. Microstructural modeling and mechanical properties computation of three-dimensional 4-directional braided composites was studied [Yang, Cui, Nie et al. (2013)]. The numerical accuracy of asymptotic homogenization method and multiscale finite element method for periodic composite materials were discussed [Dong, Nie, Yang et al. (2016)]. With the second-order correctors, the microscopic fluctuation of physical and mechanical behaviors inside the materials can be captured more accurately [Yang, Cui and Nie (2013)]. Besides, other multi-scale methods [Budarapu, Gracie, Yang et al. (2014)] have also developed to study the mechanical properties and behaviors of different materials and structures. And these methods can be used in the cases of analyzing fracture of the bone in our coming work.

However, the above mentioned unit cell models of cancellous bone are based on the assumption that all trabecular bones in the different position are either in the form of plates or rods. The microstructures in above models are simplified seriously and thus affect the accuracy of modeling results. Due to the actual structure of cancellous bone, the unit cell model structure of cancellous bone should have appropriate porosity and pore-structure. To this purpose, a periodic embedded Schwarz G surface (see Fig. 2) was introduced to describe the unit cell in this paper, since Schwarz G surface is more permeable, and it has a smooth surface to open the portion of the tissue which would facilitate the inflow of nutrients and the disposal of metabolic waste [Shin, Kim, Jeong et al. (2012)]. Thus, a new kind of unit cells, named as SG, meets the biological and mechanical requirements of cancellous bone, which is much better than other unit cell.

In this paper, a new parameterized microstructural unit cell model is established, and Schwarz G surface truly simulates the microstructure of cancellous bone. The parameterized design for the unit cell model is implemented by employing the TETGEN software. Then based on the established model, the mechanical parameters are predicted by the multiscale asymptotic method. In addition, the effect of the porosity of cancellous bone on the elastic constants is also investigated.

The remainder of this paper is outlined as follows. In Section 2, the parametric modeling process of the unit cell of cancellous bone is given. Section 3 present the formulation of the mechanical problem of cancellous bone by using multiscale asymptotic method, and the procedure of multiscale asymptotic method is also stated. Some numerical results about the mechanical properties of cancellous bone are given in Section 4. And Section 5

concludes this paper.

2 Microstructure analysis and geometric modeling of cancellous bone

2.1 Geometric modeling based on Schwarz surface

Cancellous bone is considered as the two-phase composite material, as shown in Fig. 1. At the mesoscale, the size of cancellous bone is from hundred micrometres to several millimetres, or larger, depending on the bone size, consists of a porous network of trabeculae. The mechanical property of cancellous bone depends on its morphology, which has been found to vary for different skeletal sites. In the young, the trabecular network is plexiform and dense. During ageing, as the osteoblasts are continuously compressed, trabeculae become thinner, the shape of the trabecular bone gradually changes from a plate to a rod [Hamed (2012)]. In the simulation, we assume that the cancellous bone is a symmetrical pore structure, the surface of the structure is smooth, and the two parts of the material have dual connectivity, thus ensure convenient supply and delivery of nutrients. Hyperbolic surfaces have been considered because they commonly exist in natural structures, and have sufficient porosity, high pore interconnectivity and suitable pore size, thus they are very suitable to simulate the cancellous bone as a unit cell. Amongst various hyperbolic surfaces, minimal surfaces are researched mostly. If a minimal surface has space symmetry, it is periodic in three independent directions, these surfaces are known as Triply Periodic Minimal Surfaces (TPMS).
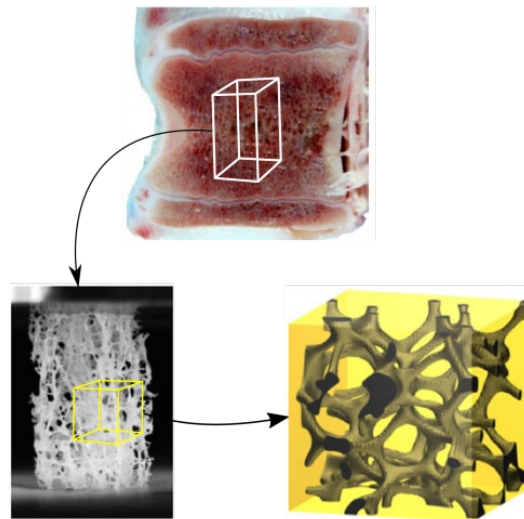

Figure 1: Specimens of trabecular bone obtained from vertebrae [Schwen (2010)]

It has been received much attentions in the recent biomaterial literatures and provide good analytic description of highly porous structures, however, there were few reports about the research on property of the cancellous bone used these TPMS.

Generally, a periodic surface can be defined as [Yoo (2013)]:

$$\phi(\mathbf{r}) = \sum_{k=1}^{K} A_k \cos[2\pi(\mathbf{h}_k \cdot \mathbf{r}) / \lambda_k + p_k] = C \tag{1}$$

Where $\mathbf{r}$ is the location vector in the Euclidean space, $\mathbf{h}_k$ is the k th lattice vector in the reciprocal space, A_k is the magnitude factor, λ_k is the wavelength of periods, p_k is the phase shift, and C is a constant. Thus specific periodic structures can be constructed based on this implicit form.

An important sub-class of TPMS is that partition space into two disjoint but intertwining regions, and these are bi-continuous. A variety of TPMS can be described, to the first order of approximation, by the following nodal equations [Yoo (2011)] the so-called Schwarz G surface can be defined as

$$\phi(x, y, z) = \sin 2\pi x \cos 2\pi y + \sin 2\pi y \cos 2\pi z + \sin 2\pi z \cos 2\pi x = C \tag{2}$$

By the Schwarz G surface, the domain is taken to be a unit cell of the periodically repeated structure. As described in formula (1), TPMS is a surface for which the mean curvature Γ is zero at every point on the surface. And then Γ divides the unit cell into the two distinct spaces, which can be represented by the zero level set of ϕ.

When $\phi(x, y, z) \leq 0$, we denote the region to be space 1, as shown in Fig. 2, and $\phi(x, y, z) \geq 0$, we denote the region to be space 2, respectively.
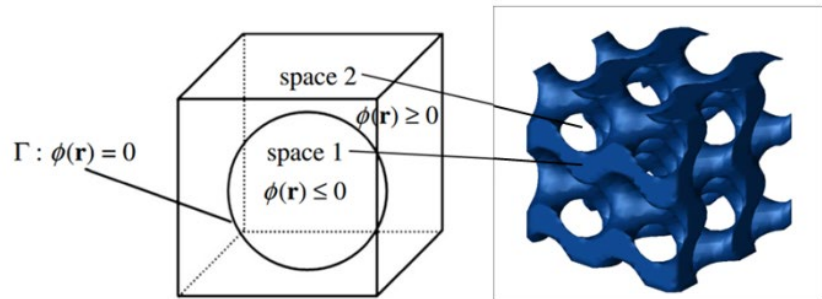

Figure 2: Schematic diagram illustrating a TPMS that divides the unit cell into two sub-spaces

There are many potential benefits of Schwarz G surface based pore architectures, so we take advantage of these newly proposed pore geometries as unit cell to simulate the cancellous bone. The following will describe beneficial properties provided by Schwarz G surface when to simulate the cancellous bone as an attractive candidate model. From the viewpoint of morphology, the unit cell generated by Schwarz G surface is very vividly to simulate the micro-structure of cancellous bone, as shown in Fig. 3.
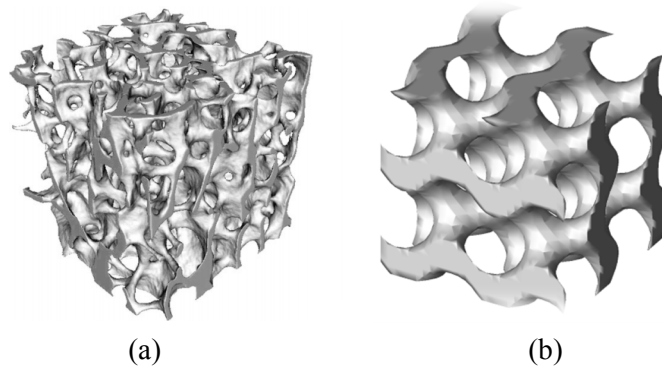
(a)   (b)

Figure 3: Real cancellous bone and corresponding unit cell. (a) 3D rendering of a bone cube from the L4 vertebral body of 66 years old male with [Parkinson and Fazzalari (2013)], (b) SG unit cell of cancellous bone

Remark 1. As a structural tissue, bone has an ideal combination of properties for its application: high stiffness, strength, fracture toughness, and light weight. Bone's excellent mechanical properties are attributed to its composite hierarchical structure. We should consider these mechanical property and biological requirements for simulating the cancellous bone. From the viewpoint of mechanical requirements, some researched results imply that the Schwarz G surface is more stable structures [Shin (2012)], and the unit cell should consider sufficient mechanical strength and stiffness for the cancellous bone to support the growing tissue.

Remark 2. From the viewpoint of biological requirements, the permeability of the unit cell should be high enough to provide superior diffusion which would facilitate the inflow of nutrients and the disposal of metabolic waste. The surface of the unit cell based on Schwarz G surface was sufficiently smooth which would be very beneficial to inflow and outflow of nutrients and metabolic waste. Micro-structure of the unit cell with a high porosity provides more space for cells to move into and begin to thrive, the unit cell based on Schwarz G surface has a large surface area which enables much more cell attachment and growth, and subsequently sufficient for tissue repair.

The aforementioned advantages help to realize self-optimizing of bone tissue and the simply form of the imply equation which saves computing time. So it is an ideal choice to generate the unit cell of cancellous bone by Schwarz G surface. Here we named this kind of unit cell as SG unit cell.

2.2 The porosity of cancellous bone

An idealized microstructural model of cancellous bone should have appropriate porosity and the pore structure, and it can easily adjust pore size and porosity of the unit cell. Now, we describe the geometry model for constructing the Schwarz G surface with a given volume fraction, the adjusting porosity is simulated by changing parameter C in formula (2). The relational between C and porosity is shown in Fig. 4.
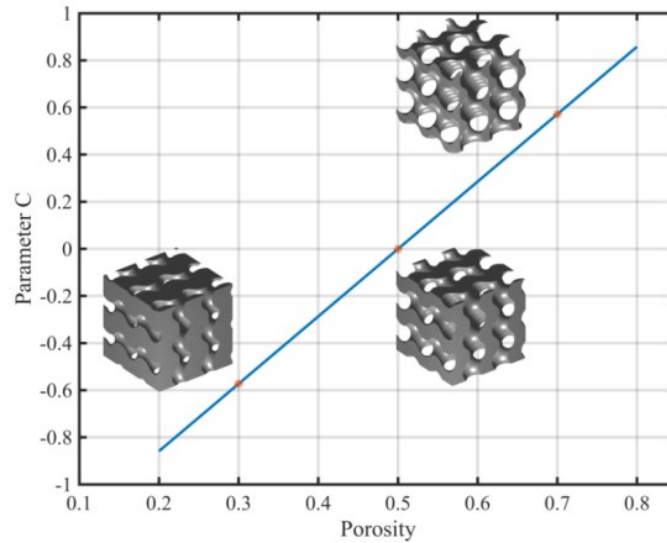
Figure 4: Funcion fittiong of the relationship between parameter C and porosity

We use the following fitting result of P against C

$$P=0.3495C+0.500 \tag{3}$$

where C is a parameter for adjusting porosity of unit cell based on the Schwarz G, P is porosity of the unit cell. Thus the porosity can be adjusted easily by changing parameter C in formula (3).

It is important that model parameters were determined expediently at numerical simulation. In this paper, model parameters are less and easy to determine, as an advantage due to extension and utilization of new geometry model. These structures will be useful to simulate bones with different ages and physiques. The different porous structures SG unit cells are shown in Fig. 5. The results corresponding to the unit cell with parameter C in the interval -0.6-0.84 are considered.

In Fig. 5, above row figures are three CT images of one health person and two patients. We can find thick cortices and dense trabecular network in the bone of young and healthy person (Fig. 5(a)). In contrast with it, the porosities of two diseased bones became larger and larger and the trabecular networks are getting looser and looser. In order to evaluate their mechanical properties, three SG unit cells are constructed by adjusting parameter C, which are arrayed below corresponding CT image. From Figs. 5(d) to 5(f), the porosities are decreasing gradually. These cells are very close to the microstructure of three kinds of cancellous bones, so they will be used for further calculation. From the viewpoint of morphology, SG unit cell is a promising structure to modelling the cancellous bone microstructure.
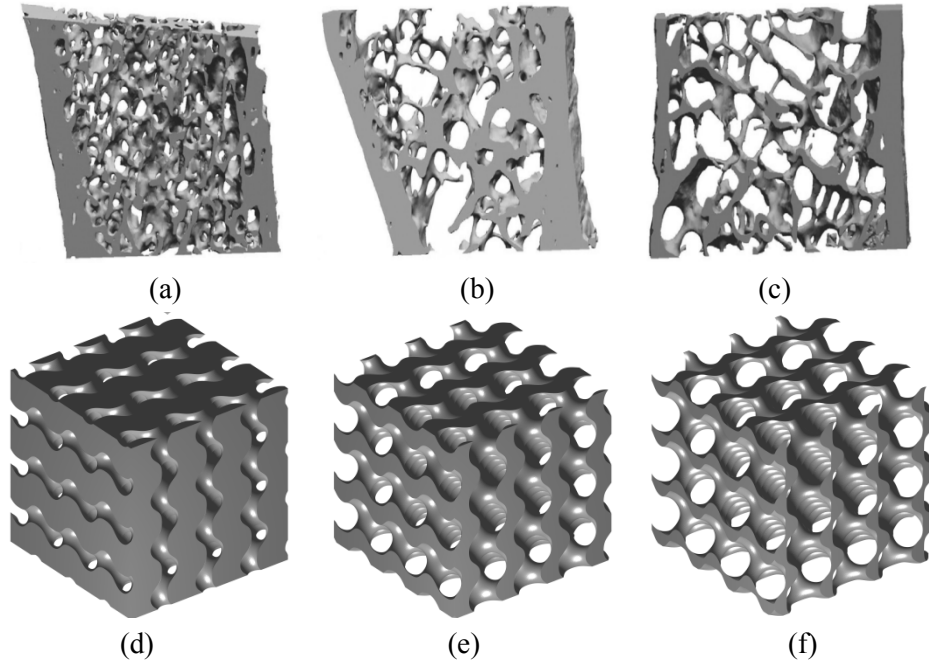
Figure 5: Micro-CT images of iliac bone and SG unit cell (a) in a young and healthy bone, (b) in a postmenopausal osteoporosis, (c) in an idiopathic osteoporosis bone [Chappard (2008)]. (d-f) the microstructure of SG unit cell with different porosity, the value of parameter C is -0.3, 0.1, and 0.79 respectively

3 Multiscale modeling of cancellous bones

In this section, the numerical modeling of cancellous bones is performed by introducing the multiscale analysis method, and its related formulation and algorithm are presented for calculating the mechanical properties of cancellous bones.

From the solid mechanics and previous microstructural modeling in Section 2, the elasticity problem of cancellous bone can be expressed as follows

$$\begin{cases} \dfrac{\partial}{\partial x_j}\left(C_{ijhk}^{\varepsilon}(x)\dfrac{1}{2}\left(\dfrac{\partial u_h^{\varepsilon}(x)}{\partial x_k} + \dfrac{\partial u_k^{\varepsilon}(x)}{\partial x_h} \right) \right) = f_i(x) & x \in \Omega \\[4mm] \mathbf{u}^{\varepsilon}(x) = \overline{\mathbf{u}}(x) & x \in \partial\Omega_1 \\[4mm] v_j C_{ijhk}^{\varepsilon}(x)\dfrac{1}{2}\left(\dfrac{\partial u_h^{\varepsilon}(x)}{\partial x_k} + \dfrac{\partial u_k^{\varepsilon}(x)}{\partial x_h} \right) = p_i(x) & x \in \partial\Omega_2 \end{cases} \tag{4}$$

where Ω denotes the macroscopic domain cancellous bones, which is composed of ε-size unit cells Y, as shown in Fig. 6; $\mathbf{u}^{\varepsilon}(x)$ denotes the displacement vector and $C_{ijhk}^{\varepsilon}(x)(i,j,h,k=1,2,3)$ the elastic coefficients.
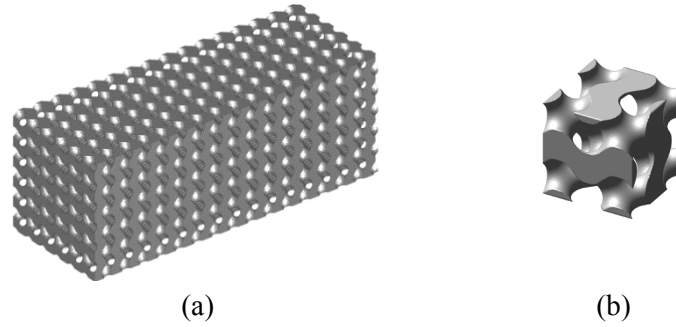
(a)   (b)

Figure 6: The cancellous bone structures (a) macrostructure Ω ; (b) unit cell Y

According to the microstructure characterization of cancellous bone in Section 2, the cancellous bone is a complex porous structure with multi-scale character. Thus, the displacement field for elasticity problem of cancellous bone depends not only on its global behaviors, but also on microscopic configurations. It hence can be expressed as $\mathbf{u}^{\varepsilon}(x) = \mathbf{u}(x, y)$, where $y = x/\varepsilon \in Y$ denotes the local coordinate on the unit cell of cancellous bone and x denotes the macroscopic coordinate, then $C_{ijhk}^{\varepsilon}(x) = C_{ijhk}(y)$.

From Yang et al. [Yang, Cui and Nie (2013)], the multiscale asymptotic expansion of the displacement can be expressed as

$$\mathbf{u}^{\varepsilon}(x) = \mathbf{u}_0(x) + \varepsilon \mathbf{N}_{\alpha_1}(y)\frac{\partial \mathbf{u}_0(x)}{\partial x_{\alpha_1}} + \varepsilon^2 \mathbf{N}_{\alpha_1 \alpha_2}(y)\frac{\partial^2 \mathbf{u}_0(x)}{\partial x_{\alpha_1}\partial x_{\alpha_2}} + \cdots \tag{5}$$

where $\mathbf{u}_0(x)$ is the macroscopic homogenized displacement defined on Ω , $\mathbf{N}_{\alpha_1}(y)$ and $\mathbf{N}_{\alpha_1 \alpha_2}(y)$ are matrix-valued local cell functions defined on the unit cell Y .

Respecting the chain rule as

$$\frac{\partial}{\partial x_i} \rightarrow \frac{\partial}{\partial x_i} + \frac{1}{\varepsilon}\frac{\partial}{\partial y_i} \tag{6}$$

and substituting (5) into (4) and matching terms of the same order of ε , we obtain that

$$\frac{\partial}{\partial x_j}\left(C_{ijhk}^\varepsilon(x)\frac{1}{2}\left(\frac{\partial u_h^\varepsilon(x)}{\partial x_k}+\frac{\partial u_k^\varepsilon(x)}{\partial x_h}\right)\right)$$

$$=\varepsilon^{-1}\left\{\frac{\partial C_{ijhk}(y)}{\partial y_j}\frac{1}{2}\left(\frac{\partial u_h^0(x)}{\partial x_k}+\frac{\partial u_k^0(x)}{\partial x_h}\right)\right.$$

$$+\frac{\partial}{\partial \xi_j}\left(C_{ijhk}(y)\frac{1}{2}\left(\frac{\partial N_{\alpha_1 hm}(y)}{\partial y_k}+\frac{\partial N_{\alpha_1 km}(y)}{\partial y_h}\right)\right)\frac{\partial u_m^0(x)}{\partial x_{\alpha_1}}\right\}$$

$$+\varepsilon^0\left\{C_{ijhk}(y)\frac{1}{2}\left(\frac{\partial^2 u_h^0(x)}{\partial x_k \partial x_j}+\frac{\partial^2 u_k^0(x)}{\partial x_h \partial x_j}\right)\right.$$

$$+C_{ijhk}(y)\frac{1}{2}\left(\frac{\partial N_{\alpha_1 hm}(y)}{\partial y_k}+\frac{\partial N_{\alpha_1 km}(y)}{\partial y_h}\right)\frac{\partial^2 u_m^0(x)}{\partial x_{\alpha_1}\partial x_j}$$

$$+\frac{\partial}{\partial y_j}\left(C_{ijhk}(y)\frac{1}{2}\left(N_{\alpha_1 hm}(y)\frac{\partial^2 u_m^0(x)}{\partial x_{\alpha_1}\partial x_k}+N_{\alpha_1 km}(y)\frac{\partial^2 u_m^0(x)}{\partial x_{\alpha_1}\partial x_h}\right)\right)$$

$$+\frac{\partial}{\partial y_j}\left(C_{ijhk}(y)\frac{1}{2}\left(\frac{\partial N_{\alpha_1\alpha_2 hm}(y)}{\partial y_k}+\frac{\partial N_{\alpha_1\alpha_2 km}(y)}{\partial y_h}\right)\right)\frac{\partial^2 u_m^0(x)}{\partial x_{\alpha_1}\partial x_{\alpha_2}}\right\}+\mathrm{O}(\varepsilon)=f_i(x)$$

(7)

And a series of equations can be obtained by equating the coefficients of the same order of ε for the above equations. And based on the theory of partial differential equations, the control equations for $N_{\alpha_1}(y)$, $N_{\alpha_1\alpha_2}(y)$ and $\mathbf{u}_0(x)$ can be determined successively.

3.1 Effective material properties model

$N_{\alpha_1 m}(y)(\alpha_1, m=1,2,3)$ satisfies the following elliptic equation

$$\begin{cases}-\frac{\partial}{\partial y_j}\left[C_{ijhk}(y)\frac{1}{2}\left(\frac{\partial N_{\alpha_1 km}(y)}{\partial y_h}+\frac{\partial N_{\alpha_1 hm}(y)}{\partial y_k}\right)\right]=\frac{\partial}{\partial y_j}\left(C_{ijm\alpha_1}(y)\right), & y\in Y\\ \int_Y N_{\alpha_1 m}(y)\mathrm{d}y=0, & N_{\alpha_1 m}(y)\in H_{per}^1(Y)\end{cases}$$

(8)

where

$$H_{per}^1(Y)=\left\{v\middle|v\in H^1(Y), v\text{ is }Y-periodic\right\}$$

From $N_{\alpha_1 m}(y)(\alpha_1, m=1,2,3)$, the effective material properties $\hat{C}_{ijhk}$ can be computed by following model

$$\hat{C}_{ijhk}=\frac{1}{|Y|}\int_Y\left(C_{ijhk}(y)+C_{ijm\alpha_1}(y)\frac{1}{2}\left(\frac{\partial N_{hmk}(y)}{\partial y_{\alpha_1}}+\frac{\partial N_{h\alpha_1 k}(y)}{\partial y_m}\right)\right)dy$$

(9)

And then the homogenized problem for the macroscopic effective displacement can be

defined as follows

$$\begin{cases} \dfrac{\partial}{\partial x_j}\left(\hat{C}_{ijhk}\dfrac{1}{2}\left(\dfrac{\partial u_{0h}(x)}{\partial x_k}+\dfrac{\partial u_{0k}(x)}{\partial x_h}\right)\right)=f_i(x) & x\in\Omega \\[4mm] \mathbf{u}_0(x)=\overline{\mathbf{u}}(x) & x\in\partial\Omega_1 \\[4mm] v_j\hat{C}_{ijhk}\dfrac{1}{2}\left(\dfrac{\partial u_{0h}(x)}{\partial x_k}+\dfrac{\partial u_{0k}(x)}{\partial x_h}\right)=p_i(x) & x\in\partial\Omega_2 \end{cases} \tag{10}$$

3.2 Microscopic stress computational model

$\mathbf{N}_{\alpha_1\alpha_2 m}(y)(\alpha_1,\alpha_2,m=1,2,3)$ are solutions of the following problem

$$\begin{cases} -\dfrac{\partial}{\partial y_j}\left[C_{ijhk}(y)\dfrac{1}{2}\left(\dfrac{\partial\mathbf{N}_{\alpha_1\alpha_2 km}(y)}{\partial y_h}+\dfrac{\partial\mathbf{N}_{\alpha_1\alpha_2 hm}(y)}{\partial y_k}\right)\right]=\dfrac{\partial}{\partial y_j}\left(C_{ijk\alpha_2}(y)\mathbf{N}_{\alpha_1 km}(y)\right) \\[4mm] +C_{i\alpha_1 kj}(y)\dfrac{\partial\mathbf{N}_{\alpha_2 km}(y)}{\partial y_j}+C_{i\alpha_1 m\alpha_2}(y)-\hat{C}_{i\alpha_1 m\alpha_2}, \quad y\in Y \\[4mm] \displaystyle\int_Y \mathbf{N}_{\alpha_1\alpha_2 m}(y)\,\mathrm{d}y=0, \quad \mathbf{N}_{\alpha_1\alpha_2 m}(y)\in H^1_{per}(Y) \end{cases} \tag{11}$$

In actual engineering calculation, the multiscale asymptotic expansion of the displacement can be taken as

$$\mathbf{u}^{\varepsilon,2}(x)=\mathbf{u}_0(x)+\varepsilon\mathbf{N}_{\alpha_1}\left(y\right)\dfrac{\partial\mathbf{u}_0(x)}{\partial x_{\alpha_1}}+\varepsilon^2\mathbf{N}_{\alpha_1\alpha_2}\left(y\right)\dfrac{\partial^2\mathbf{u}_0(x)}{\partial x_{\alpha_1}\partial x_{\alpha_2}} \tag{12}$$

Then, the strains inside the structure Ω can be calculated by the following formula

$$\begin{aligned} \varepsilon_{hk}(x,y)=&\dfrac{1}{2}\left(\dfrac{\partial u_h^0(x)}{\partial x_k}+\dfrac{\partial u_k^0(x)}{\partial x_h}\right)+\sum_{l=1}^2\varepsilon^{l-1}\sum_{<\boldsymbol{\alpha}>=l}\dfrac{1}{2}\left[\dfrac{\partial N_{\boldsymbol{\alpha}hm}(y)}{\partial y_k}+\dfrac{\partial N_{\boldsymbol{\alpha}km}(y)}{\partial y_h}\right]D_{\boldsymbol{\alpha}}^l u_m^0(x) \\ &+\sum_{l=1}^2\varepsilon^l\sum_{<\boldsymbol{\alpha}>=l}\dfrac{1}{2}\left[N_{\boldsymbol{\alpha}hm}(y)D_{\boldsymbol{\alpha}k}^{l+1}u_m^0(x)+N_{\boldsymbol{\alpha}km}(y)D_{\boldsymbol{\alpha}h}^{l+1}u_m^0(x)\right] \end{aligned} \tag{13}$$

And from Hooke's law, the stresses inside Ω are calculated by

$$\sigma_{ij}(x,y)=C_{ijhk}(y)\varepsilon_{hk}(x,y) \tag{14}$$

Remark 3. Substituting $\mathbf{u}^\varepsilon(x)-\mathbf{u}^{\varepsilon,2}(x)$ into the original problem (4) and considering the chain rule (6), it yields

$$\dfrac{\partial}{\partial x_j}\left(C_{ijhk}^\varepsilon(x)\dfrac{1}{2}\left(\dfrac{\partial}{\partial x_k}\left(u_h^\varepsilon(x)-u_h^{\varepsilon,2}(x)\right)+\dfrac{\partial}{\partial x_h}\left(u_k^\varepsilon(x)-u_k^{\varepsilon,2}(x)\right)\right)\right)=O(\varepsilon) \tag{15}$$

It can be concluded from (15) that the multiscale solution (12) are equivalent to exact solutions of problem (4) with order $O(\varepsilon)$ in nearly pointwise sense. In fact, the solution $\mathbf{u}^{\varepsilon,2}(x)$ satisfies the stress equilibrium equation nearly anywhere inside the structures in

pointwise sense and thus it can offer satisfactory local stress state, which is very important in the practical engineering computation.

3.3 Computational implement of multiscale method

3.3.1 Finite element computation of effective material parameters

The FE solutions of cell functions $N_{\alpha_1}(y)(\alpha_1 = 1,2,3)$ can be obtained by solving the following FE virtual work equation on unit cell Y which is equivalent to (8)

$$\int_Y C_{ijhk}(y)\frac{1}{2}\left(\frac{\partial \mathbf{N}^{h_1}_{\alpha_1 km}(y)}{\partial y_h}+\frac{\partial \mathbf{N}^{h_1}_{\alpha_1 hm}(y)}{\partial y_k}\right)\frac{\partial \upsilon}{\partial y_j}dy = -\int_Y C_{ijm\alpha_1}(y)\frac{\partial \upsilon}{\partial y_j}dy, \quad \forall \upsilon \in V^{h_1}(Y) \tag{16}$$

where $V^{h_1}(Y)\subseteq H_0^1(Y)$ denotes the FE space of 1-square Y, Y is partitioned into FE set $V^{h_1}(Y)$ of finite elements, h_1 is the mesh size. Then, the FE approximation $\hat{C}^{h_1}_{ijhk}(y)$ of homogenized elastic coefficients can be evaluated as follows

$$\hat{C}^{h_1}_{ijhk}(y) = \frac{1}{|Y|}\int_Y\left(C_{ijhk}(y)+C_{ijm\alpha_1}(y)\frac{1}{2}\left(\frac{\partial \mathbf{N}^{h_1}_{hmk}(y)}{\partial y_{\alpha_1}}+\frac{\partial \mathbf{N}^{h_1}_{h\alpha_1 k}(y)}{\partial y_m}\right)\right)dz \tag{17}$$

Similar to (16), local cell problems (11) can be solved to obtain $N^{h_1}_{\alpha_1\alpha_2}(y)$.

3.3.2 Finite element computation of micro and macro stresses

The FE solution of the homogenized problem (10) is the solution of following FE virtual work equations associated with homogenized coefficient (9) on Ω

$$\int_\Omega \hat{C}^{h_1}_{ijhk}\frac{1}{2}\left(\frac{\partial u^{h_0}_{0h}(x)}{\partial x_k}+\frac{\partial u^{h_0}_{0k}(x)}{\partial x_h}\right)\frac{\partial w}{\partial x_j}dx = \int_\Omega f_i(x)wdx+\int_{\Gamma_2}p_i(x)wdS, \quad \forall w\in V^{h_0}(\Omega) \tag{18}$$

where V^{h_0} denotes the FE space with mesh size h_0 on homogenized domain Ω.

Finally, according to (13) and applying the FE solutions of microscale and macroscale problems, the multiscale FE approximation solutions of stresses on the macroscale and microscale can be obtained as follows

$$\sigma^0_{ij}(x,y) = \hat{C}^{h_1}_{ijhk}(y)\frac{1}{2}\left(\frac{\partial u^{0h_0}_h(x)}{\partial x_k}+\frac{\partial u^{0h_0}_k(x)}{\partial x_h}\right) \tag{19}$$

$$\begin{aligned}
\sigma^2_{ij}(x,y) &= \hat{C}^{h_1}_{ijhk}(y)\frac{1}{2}\left(\frac{\partial u^{0h_0}_h(x)}{\partial x_k}+\frac{\partial u^{0h_0}_k(x)}{\partial x_h}\right) \\
&+\hat{C}^{h_1}_{ijhk}(y)\sum_{l=1}^2\varepsilon^{l-1}\sum_{<\alpha>=l}\frac{1}{2}\left[\frac{\partial N^{h_1}_{\alpha hm}(y)}{\partial y_k}+\frac{\partial N^{h_1}_{\alpha km}(y)}{\partial y_h}\right]D^l_\alpha u^{0h_0}_m(x) \\
&+\hat{C}^{h_1}_{ijhk}(y)\sum_{l=1}^2\varepsilon^l\sum_{<\alpha>=l}\frac{1}{2}\left[N^{h_1}_{\alpha hm}(y)D^{l+1}_{\alpha k}u^{0h_0}_m(x)+N^{h_1}_{\alpha km}(y)D^{l+1}_{\alpha h}u^{0h_0}_m(x)\right]
\end{aligned} \tag{20}$$

3.3.3 The flowchart of the multiscale method

The flow chart of the algorithm for the multiscale method for prediction of the mechanical properties of cancellous bone is given in Tab. 1.

Table 1: Flowchart for computing the mechanical properties of cancellous bone

| Input	C_{ijhk} , Porosity, elastic properties of cancellous bone
①	Generate the geometrical structure of the microscopic cell Y, and then partition it into finite element meshes (Fig. 7).
②	Compute the FE solutions of $N_{\alpha_1}(y)$ according to the problem (8) with given material properties based on the FE meshes of unit cell Y. And then evaluate the effective homogenized coefficient $\hat{C}_{ijhk}$ by the formula (9).
③	According to the homogenized parameters obtained in step ②, the homogenized solution $\mathbf{u}_0(x)$ is obtained by solving (10) on homogenized domain Ω.
④	Using the same meshes as in Step 1, we evaluate $N_{\alpha_1\alpha_2}(y)$ by solving the cell problems (11) on unit cell Y.
⑤	Compute the high-order partial derivatives of $\mathbf{u}_0(x)$ by the average technique on relative elements.
⑥	From (12), the multiscale solution of displacement field is evaluated. Further, the distributions of strain and stress fields in the microscale can be obtained from (13) and (14), respectively.
Output	$\hat{C}_{ijhk}$ and the stresses

(a)   (b)
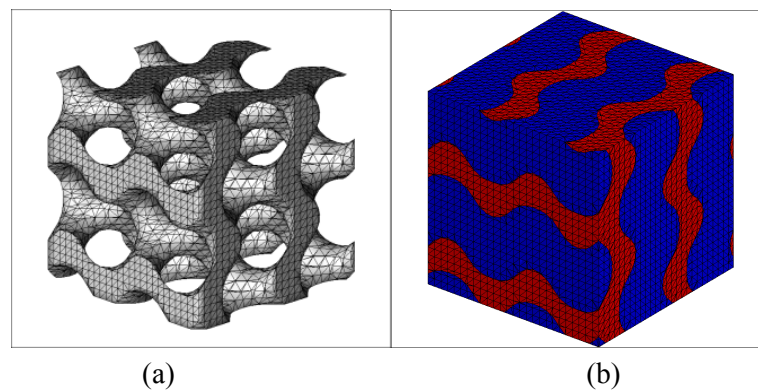
Figure 7: FE meshes of the unit cell of cancellous bone. The meshes of (a) Solid phase and (b) the entire unit cell

Remark 4. Due to the complexity of the geometry model of cancellous bone, the precision of the multiscale analysis method is greatly influenced by the quality of the FE meshes. In this paper, the TETGEN software package is used to generate the FE meshes of the unit cell. The geometry model of the unit cell generated by the MATLAB code is imported into the TETGEN software, and then the unit cell with the porosity of 21% was meshed by 112413 tetrahedral elements as shown in Fig. 7.

4 Numerical examples

In this section, some numerical examples are given to show the effectiveness of the numerical method for predicting the mechanical propertied of cancellous bone.

Mechanical properties and volume fractions of cancellous bone components play an important role in its overall behavior. Cancellous bone can be seen as a composite of trabecular bone and bone marrow, and their material properties used in this section are summarized in Tab. 2. Moreover, all components are assumed to have linear elastic and isotropic behavior. We consider the porosity within the scope of 0.3~0.8 and it can be controlled by only one parameter, as showed in many literature, it needs more parameters or different unit cells model in order to investigate the extensive porosity scope, this is one of the obvious advantages of the newly used unit cell.

Table 2: Properties of bone components selected [Hamed, Lee and Jasiuk (2010)]

Material	Elastic modulus (GPa)	Poission's ratio	Volume fraction (%)
Trabecular bone	22	0.32	30~80
Bone marrow	2.3	0.45	

4.1 Effective stiffness parameters

Our analysis has shown significant linear correlation between volume fraction ratio and the Young's modulus, as shown in Fig. 8. Dependence of Young's modulus and shear modulus on porosity is a smooth, monotonically decreasing function, while Poisson's ratio shows opposite behavior and it increases with increasing porosity. Young's modulus takes the values in the interval 0.753-3.029 Gpa, the shear modulus 384.38-1381.32 Gpa and Poisson's ratio 0.256-0.274 for the porosity from 0.290-0.795. The results mentioned above show that the effective mechanical properties of the cancellous are within the range of macroscopic reported in literature [Ilic, Hackl and Gilbert (2009); Hayes (1985)]. Compared previous studies to idealized cancellous bone models, these results are reasonable.
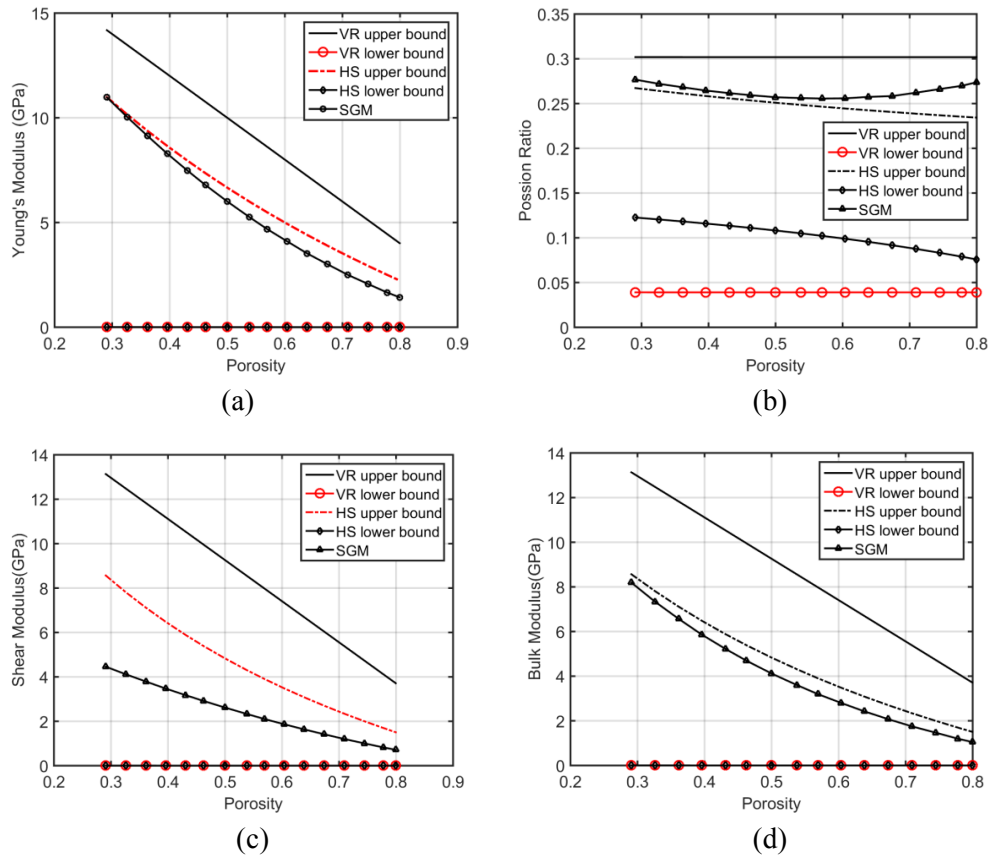
Figure 8: Change of effcetive material parameters versus porosity for the biphasic material. (a) Young's modulus(b) Poisson's ratio (c) shear modulus (d) bulk modulus

Besides, results of SG unit cell are compared with those obtained by different analytical methods, including Voight-Reuss bounds (VR) and Hashin-Shtrikman bounds (HS), Young's modulus, shear modulus, Poisson's ratio and bulk modulus are evaluated respectively, and their variation curves are shown in Fig. 8. It is found that mechanical properties are located between the upper bound and the lower bound of the HS and the VR at entire interval. All the results show that SG unit cell is valid to predict the effective mechanical properties of cancellous bone.

Table 3: Comparison of modelling results for effective material properties of cancellous bone obtained by SG unit cell (SGM) and document [Podshivalov, Fischer and Yoseph (2011)] (DOC 1) [Helgason, Schileo, Taddei et al. (2008)] (DOC 2)

Model	Porosity	E_{11}	E_{22}	E_{33}	ν_{12}	ν_{31}	ν_{23}	G_{23}	G_{31}	G_{12}
SGM	0.273	10.977	10.967	11.008	0.277	0.276	0.276	4.458	4.462	4.459
DOC1	0.273	13.1	13.2	12.6	0.289	0.275	0.273	5.0	5.1	5.1
SGM	0.453	6.788	6.786	6.833	0.259	0.257	0.257	2.918	2.921	2.919
DOC1	0.453	7.8	7.4	7.8	0.266	0.245	0.218	2.9	2.9	2.9
SGM	0.571	4.688	4.679	4.716	0.256	0.254	0.254	2.104	2.106	2.106
DOC1	0.571	5.0	4.4	3.9	0.263	0.229	0.200	1.7	1.8	1.8
SGM	0.630	3.524	3.519	3.555	0.257	0.255	0.255	1.636	1.638	1.638
DOC2	0.630	3.739	-----	-----	-----	-----	-----	-----	-----	-----
DOC1	0.630	3.8	3.3	2.8	0.267	0.222	0.200	1.3	1.3	1.3
SGM	0.658	3.009	3.004	3.028	0.258	0.257	0.256	1.418	1.417	1.479
DOC2	0.658	3.325	-----	-----	-----	-----	-----	-----	-----	-----
DOC1	0.658	3.2	2.8	2.2	0.269	0.222	0.196	1.1	1.1	1.1
SGM	0.709	2.503	2.500	2.523	0.262	0.259	0.259	1.203	1.203	1.202
DOC2	0.709	2.614	-----	-----	-----	-----	-----	-----	-----	-----
SGM	0.745	2.043	2.037	2.063	0.247	0.243	0.243	1.015	1.013	1.015
DOC2	0.745	2.147	-----	-----	-----	-----	-----	-----	-----	-----
SGM	0.799	1.425	1.419	1.436	0.274	0.271	0.271	0.715	0.717	0.717
DOC2	0.799	1.506	-----	-----	-----	-----	-----	-----	-----	-----

According to the proposed algorithm, the effective material properties are calculated for geometric models and it presented as a function of porosity (0.273-0.799) in Tab. 3. Comparing the SGM results with the experimental data [Podshivalov, Fischer and Yoseph. (2011)], the results (porosity from 0.3 to 0.6) agree with the results obtained by [Podshivalov, Fischer and Bar-Yoseph (2011)]. In addition, Young' modulus are compared with the experimental data [Helgason, Schileo, Taddei et al. (2008)], there is a good agreement between experimental data and SGM results. Compared previous studies to idealized cancellous bone models, to achieve the same calculation results, the method used in this paper is simple to model and more computationally efficient. The results demonstrate that the present model is applicable and the multiscale asymptotic method is effective to predict the mechanical properties of the cancellous bone.

The effective material parameters were mostly investigated as pure skeleton structure [Zysset (2003); Hoffler, Kozloff, Zysset et al. (2000); Zysset, Guo, Hoffler et al. (1999)]. For the purpose of comparison, the calculations are repeated for the unit cell without bone marrow. As shown in Fig. 9, the maximum relative error is less than about 0.025%. The results show that the bone marrow does not significantly influence to the values of mechanical properties of cancellous bone, thus, the bone marrow can be neglected during modeling and computing, but it may affect mechanical property through bone remodeling.
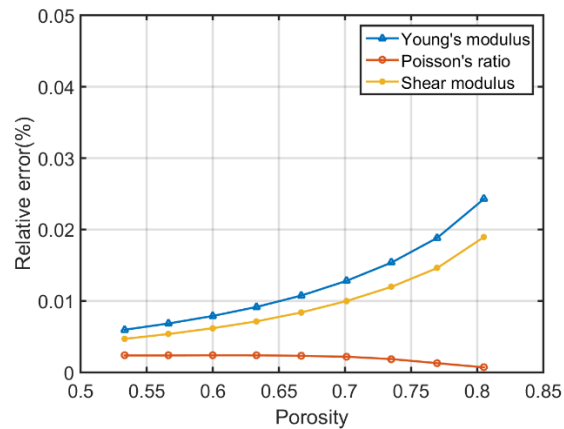

Figure 9: Relative error of material parameters over porosity between biphasic material and the dry skeleton

4.2 Microscopic stress distributions

In order to calculate the stress in the microstructure, a cancellous bone, which is cubic structure with side length of 3 cm, is investigated. The material properties are listed in Tab. 2 and the porosity of cancellous bone is 53%. The cubic structure is clamped on its bottom surface and exposed to a compressive force which is 75N on the top surface, as shown in Fig. 10. Fig. 11 shows the maximum shear stress distributions in the cells at z=0.8 cm and 2.2cm, respectively. It can be found that the stresses in cells have a marked fluctuation. As for the second-order correctors of the multiscale asymptotic method, the microscopic fluctuation of physical and mechanical behaviors inside the bone can be captured more

accurately, this method can be used in the cases of analyzing fracture of the bone in the coming work. The other significant relationships between density and the elastic properties can be computed by SG unit cell, it is important to bone remodeling.
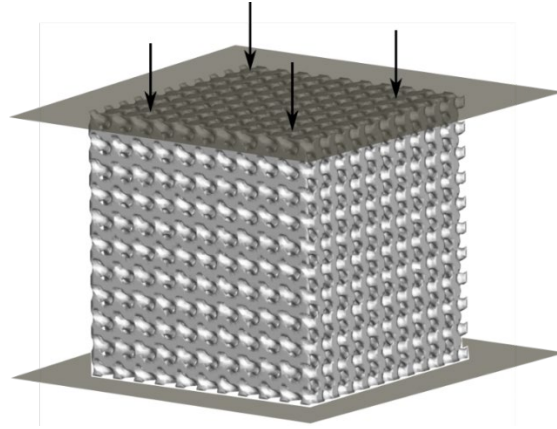

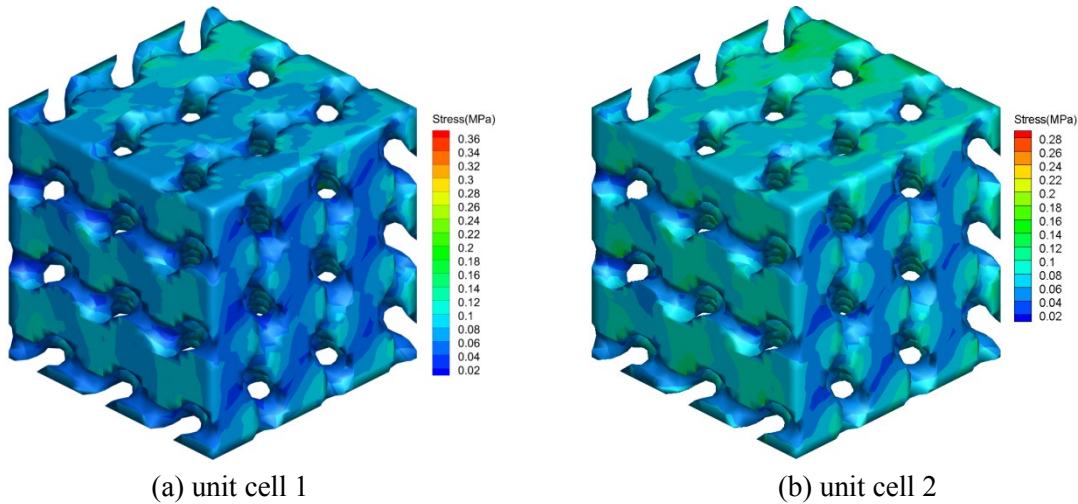**Figure 10:** Compression test simulation for the cancellous bone structure

(a) unit cell 1   (b) unit cell 2

Figure 11: Maximum shear stress in local unit cell of cancellous bone

5 Conclusions

In this paper, a new microstructural unit cell model is established and the multiscale analysis method is used to predict the mechanical properties of cancellous bone, including the stiffness parameters and stress distributions. The geometric model of unit cell is established by introducing Schwarz surface and implemented by the MATLAB code. And this unit model truly simulates the microstructure of cancellous bone. The pores in the unit cell are connected and the porosity can range from 30% to 80%, which satisfies the main biological characteristics of cancellous bone. Based on the unit cell model, Poisson's ratio, shear modulus and elastic modulus, as well as the microscopic stress distribution of

cancellous bone are predicted by the multiscale analysis method. The good agreement between the calculated results and experimental data demonstrates that the established unit cell model is applicable and the multiscale analysis method is valid to predict the mechanical properties of cancellous bone. The results also show that the multiscale method can accurately capture the microscopic characteristics of cancellous bone. Moreover, the relation between the porosity and elastic constants is studied, and the results show that it is an important factor affecting the mechanical properties.

References

Arabnejad K.; Pasini, S. D. (2013): Fatigue design of a mechanically biocompatible lattice for a proof-of-concept femoral stem. *Journal of the Mechanical Behavior of Biomedical Materials*, vol. 22, pp. 65-83.

Al-Ketan, O.; Adel, A. M.; Abu Al-Rub, R. K. (2017): Mechanical properties of periodic interpenetrating phase composites with novel architected microstructures. *Composite Structures*, vol. 176, pp. 9-19.

Budarapu, P. R.; Gracie, R.; Bordas, S. P. A.; Rabczuk, T. (2014): An adaptive multiscale method for quasi-static crack growth. *Computational Mechanics*, vol. 53, pp. 1129-1148.

Budarapu, P. R.; Gracie, R.; Yang, S. W.; Zhuang, X. Y.; Rabczuk, T. (2014): Efficient coarse graining in multiscale modeling of fracture. *Theoretical and Applied Fracture Mechanics*, vol. 69, pp.126-143.

Basaruddin, K. S.; Takano, N.; Nakano, T. (2015): Stochastic multi-scale prediction on the apparent elastic moduli of trabecular bone considering uncertainties of biological apatite (BAp) crystallite orientation and image-based modelling. *Computer Methods in Biomechanics and Biomedical Engineering*, vol. 18, pp. 162-174.

Barak, M. M.; Black, M. A. (2018): A novel use of 3D printing model demonstrates the effects of deteriorated trabecular bone structure on bone stiffness and strength. *Journal of the Mechanical Behavior of Biomedical Materials*, vol. 78, pp. 455-464.

Cui, J. Z.; Shin, T. M.; Wang, Y. L. (1999): Two-scale analysis method for bodies with small periodic configuration. *Structural Engineering and Mechanics*, vol. 7, no. 6, pp. 601-614.

Cui, J. Z.; Yu, X. G. (2006): A two-scale method for identifying mechanical parameters of composite materials with periodic configuration. *Acta Mechanica Sinica*, vol. 22, no. 6, pp. 581-594.

Chappard, D.; Basle, M. F.; Legrand, E.; Audran, M. (2008): Trabecular bone microarchitecture: a review. *Morphologie*, vol. 92, pp. 162-170.

Dong, H.; Nie, Y. F.; Yang, Z. H.; Zhang, Y.; Wu, Y. T. (2016): The numerical accuracy analysis of asymptotic homogenization method and multiscale finite element method for

periodic composite materials. *Computer Modeling in Engineering & Sciences*, vol. 111, pp. 395-419.

Fritsch, A., Hellmich, C., Dormieux, L. (2009): Ductile sliding between mineral crystals followed by rupture of collagen crosslinks: experimentally supported micromechanical explanation of bone strength. *Journal of Theoretical Biology*, vol. 260, pp. 230-252.

Hamed, E.; Jasiuk, I.; Yoo, A.; Lee, Y. H.; Liszka, T. (2012): Multi-scale modelling of elastic moduli of trabecular bone. *Journal of the Royal Society Interface*, vol. 9, pp. 1654-1673.

Beaupre, G. S.; Hayes, W. C. (1985): Finite element analysis of a three-dimensional open-celled model for trabecular bone. *Journal of Biomechanical Engineering*, vol. 107, pp. 249-258.

Hosokawa, A. (2006): Ultrasonic pulse waves in cancellous bone analyzed by finite-difference time-domain methods. *Ultrasonics*, vol. 44, pp. 227-231.

Hamed, E.; Lee, Y.; Jasiuk, I. (2010): Multiscale modeling of elastic properties of cortical bone. *Acta Mechanica*, vol. 213, pp. 131-154.

Helgason, B. P.; Schileo, E.; Taddei, E.; Brynjolfsson, F.; Viceconti, M. S. (2008): Mathematical relationships between bone density and mechanical properties: a literature review. *Clinical Biomechanics*, vol. 23, no. 2, pp. 135-146.

Hoffler, C. E.; Moore, K. E.; Kozloff, K.; Zysset, P. K.; Brown, M. B. et al. (2000): Heterogeneity of bone lamellar-level elastic moduli. *Bone*, vol. 26, no. 6, pp. 603-609.

Huang, Z. Q.; Nie, Y. F.; Yang, Z. H.; Li, Y. Q.; Guo, N. P. (2017): Multiscale modeling for mechanical properties of cancellous bone based on the schwarz surface. *3rd International Conference on Mechatronics and Mechanical Engineering*, vol. 95.

Hamdiab, K. M.; Ghasemi, H.; Zhuang, X. Y.; Alajlana, N.; Rabczuk, T. (2018): Sensitivity and uncertainty analysis for flexoelectric nanostructures. *Computer in Methods Applied Mechanics and Engineering*, vol. 337, pp. 95-109.

Ilic, S.; Hackl, K.; Gilbert, R. (2009): Application of the multiscale FEM to the modeling of cancellous bone. *Biomechanics and Modeling in Mechanobiology*, vol. 9, pp. 87-102.

Jaziri, A.; Rahmoun, J.; Naceur, H.; Drazetic, P.; Markiewicz, E. (2012): Multi-scale modelling of the trabecular bone elastoplastic behaviour under compression loading. *European Journal of Computational Mechanics*, vol. 21, pp. 254-269.

McElhaney, J. H.; Fogle, J. L.; Melvin, J. W.; Haynes, R. R.; Roberts, V. L. et al. (1970): Mechanical properties of cranical bone. *Journal of Biomechanics*, vol. 3, pp. 495-511.

Nikolov, S., Raabe, D. (2008): Hierarchical modeling of the elastic properties of bone at submicron scales: the role of extrafibrillar mineralization. *Biophysical Journal*, vol. 94, pp. 4220-4232.

Podshivalov, L.; Fischer, A.; Bar-Yoseph, P. Z. (2011): Multiscale FE method for analysis of bone micro-structures. *Journal of the Mechanical Behavior of Biomedical Materials*, vol. 4, pp. 888-899.

Sansalone, V.; Naili, S.; Desceliers, C. (2014): A stochastic homogenization approach to

estimate bone elastic properties. *Comptes Rendus Mathematique*, vol. 342, no. 5, pp. 326-333.

Parkinson, I. H.; Fazzalari, N. L. (2013): Characterisation of trabecular bone structure. vol. 5, pp. 31-51.

Schwen, L. O. (2010): *Composite Finite Elements for Trabecular Bone Microstructures (Ph.D. Thesis)*. University of Bonn, Germany.

Shin, J.; Kim, S.; Jeong, D.; Lee, H. G.; Lee, D. (2012): Finite element analysis of Schwarz P surface pore geometries for tissue-engineered scaffolds. *Mathematical Problems in Engineering*, vol. 2012, pp. 1-13.

Vu-Bac, N.; Silani, M.; Lahmer, T.; Zhuang, X.; Rabczuk, T. (2015): A unified framework for stochastic predictions of mechanical properties of polymeric nanocomposites. *Computational Materials Science*, vol. 96, pp. 520-535.

Yang, Z. Q.; Cui, J. Z.; Nie, Y. F.; Ma, Q. (2012): The second-order two-scale method for heat transfer performances of periodic porous materials with interior surface radiation. *Computer Modeling in Engineering & Sciences*, vol. 88, no. 5, pp. 419-442.

Yang, Z. H.; Cui, J. Z.; Nie, Y. F.; Wu, Y. T.; Yang, B. et al. (2013) Microstructural modeling and second-order two-scale computation for mechanical properties of 3D 4-directional braided composites. *Computers, Materials & Continua*, vol. 38, pp. 175-194.

Yang, Z. H.; Cui, J. Z.; Nie, Y. F. (2013): Microstructural modeling and second-order two-scale computation for mechanical properties of 3D 4-directional braided composites. *Computers, Materials & Continua*, vol. 38, pp. 175-194.

Yoo, D. J. (2013): New paradigms in hierarchical porous scaffold design for tissue engineering. *Materials Science & Engineering C-Materials for Biological Applications*, vol. 33, no. 3, pp. 1759-1772.

Yoo, D. J. (2011): Computer-aided porous scaffold design for tissue engineering using triply periodic minimal surfaces. *International Journal of Precision Engineering and Manufacturing*, vol. 12, pp. 61-71.

Zysset, P. (2003): A review of morphology-elasticity relationships in human trabecular bone: theories and experiments. *Journal of Biomechanics*, vol. 36, no. 10, pp. 1469-1485.

Zysset, P. K.; Guo, X. E.; Hoffler, C. E.; Moore, K. E.; Goldstein, S. A. (1999): Elastic modulus and hardness of cortical and trabecular bone lamellae measured by nanoindentation in the human femur. *Journal of Biomechanics*, vol. 32, pp. 1005-1012.